Interaction of wide-band-gap single crystals with 248-nm excimer laser radiation. XI. The effect of water vapor and temperature on laser desorption of neutral atoms from sodium chloride

K. H. Nwe, S. C. Langford, and J. T. Dickinson[a)]
Physics Department, Washington State University, Pullman, Washington 99164-2814

W. P. Hess
Pacific Northwest National Laboratory, P.O. Box 999, Richland, Washington 99352

(Received 26 July 2004; accepted 9 November 2004; published online 20 January 2005)

We show that low partial pressures of water vapor (10^{-5} Pa) dramatically increase the intensity of neutral Na and Cl emissions from cleaved, single-crystal NaCl during pulsed laser irradiation at 248 nm (KrF excimer). The time-of-flight distributions of these emissions are consistent with thermal desorption from laser-heated surfaces. Significantly, introducing water vapor lowers the particle velocities and thus the effective surface temperature during emission. Transmission measurements confirm that laser absorption is reduced in the presence of water vapor. The Arrhenius analysis of the emission intensities and effective temperatures show reduced activation energies in the presence of water vapor, which more than compensate for the vapor-induced reduction in laser absorption and surface temperature. Atomic force and scanning electron microscopy of the irradiated surfaces show evidence for accelerated monolayer-scale erosion in the presence of water vapor. A mechanism for the effect of water on these emission and erosion processes is proposed and discussed. © *2005 American Institute of Physics*. [DOI: 10.1063/1.1847697]

I. INTRODUCTION

Defect production and desorption involving electronic excitations have important applications in optics and electronics. In many material systems, simultaneous electronic excitation and exposure to aggressive chemicals can accelerate etching in a controlled fashion. In the commercial silicon/silicon oxide system, these chemicals (e.g., fluorine compounds) can be extremely reactive. In this work, we demonstrate dramatically increased rates of laser-induced neutral particle desorption and surface erosion on single-crystal sodium chloride in the presence of low partial pressures (10^{-5} Pa) of water vapor. Water is a relatively inert and safe chemical, but one with significant reactivity in a number of important material systems, particularly when it absorbs dissociatively.

Electronic excitations in the alkali halides have been well studied.[1–4] These excitations can lead to the desorption of halogen atoms and molecules, either by diffusion of halogen-excess defects to the surfaces or by the decay of excitations at the surface.[5–7] In the presence of surface defects, electronic excitations can yield both alkali and halogen emission, often yielding layer-by-layer material removal in the early stages of irradiation.[8–11] These processes are readily studied by using relatively low fluxes of energetic particles or photons, where bulk sample heating is negligible and laser ablation (plasma formation) is totally avoided.

Emissions during pulsed, ultraviolet laser radiation can be complicated by rapidly changing defect densities in the early stages of irradiation. In recent work, we showed that single-crystal NaCl develops a highly defective layer along the surface during the first five or ten pulses of 248-nm excimer laser radiation at fluences near 100 mJ/cm^2.[12,13] These laser fluences are well below those required to produce optical breakdown and thus probe processes much gentler than those that yield visible plasmas or plumes.[14] Nevertheless, the effective surface temperatures can briefly exceed the boiling point of sodium chloride without producing obvious meltlike surface features.[13]

In this work, we show that low partial pressures of water vapor ($\leqslant 10^{-5}$ Pa) can dramatically enhance the emission of neutral Na and Cl from single-crystal sodium chloride at comparable laser fluences. The effect of laser fluence on emission intensities is consistent with a transient, thermally assisted process taking place toward the end of the laser pulse, when the surface reaches its maximum temperature.[12,13] This temperature is estimated by fitting the particle time-of-flight (TOF) curves to the Maxwell–Boltzmann distribution for effusing particles. The enhanced emission intensities in the presence of water vapor are attributed to a decrease in the activation energy of this transient process. This enhancement occurs *despite* reductions in the effective surface temperature and laser absorption in the presence of water vapor. The intense emissions observed in the presence of water vapor are associated with correspondingly large erosion features in scanning electron and atomic force microscope images of the irradiated surfaces.

II. EXPERIMENT

The single-crystal NaCl employed is this work was a cleavable variety obtained from Almaz Optics (West Berlin, New Jersey). After cleaving, the samples were mounted in a vacuum system with a base pressure below 10^{-7} Pa. Pulsed

[a)]Electronic mail: jtd@wsu.edu

laser radiation at 248 nm was provided by a Lambda Physik Lextra 200 excimer laser (KrF excimer, 5-eV photons, 30-ns pulse width). In this work, the sample temperature was controlled by resistively heating the sample holder while monitoring its temperature with a chromel-alumel thermocouple welded to the holder. After each change in temperature, 20 min were allowed for the sample to equilibrate with the sample holder prior to data acquisition. Water vapor was introduced through an UHV leak valve from a reservoir of degassed, de-ionized water. By rapidly opening the leak valve, the partial pressure of water vapor could be increased with time constants on the order of a few tenths of a second. Quickly closing the valve resulted in a much slower drop in the partial pressure of water (typically 2–4 s) due to the well documented behavior of water vapor in a vacuum system with finite pumping speed.[15]

The peak surface temperature reached during the laser pulse, T, was estimated from the time of flight of thermally desorbed particles. At particle removal rates well below a monolayer per pulse, the time of flight of thermally desorbed particles can be modeled by a delta function source of effusing particles with Maxwell–Boltzmann velocity distributions. When N particles are emitted from the surface, the signal detected with the quadrupole ionizer mounted at a distance d from the surface, with d much greater than the dimensions of the ionizer, is given by

$$I(t) = \left(\frac{m}{2\pi kT}\right)^{3/2} \frac{\alpha NVd}{(t-t')^4} \exp\left(\frac{-md^2}{2kT(t-t')^2}\right), \quad (1)$$

where α is the ionizer/mass filter efficiency, V is the ionizer volume, t' is the time required for the ionized neutral to pass through the mass filter to the detector, and k is the Boltzmann constant.

Surface structures produced by laser radiation were characterized by a JEOL JSM 6400 scanning electron microscope and a Digital Instruments. Nanoscope III multimode scanning probe microscope. Atomic force imaging employed commercial Si_3N_4 cantilevers (tip radii typically 40 nm) in the contact mode.

III. RESULTS

A. Neutral emission in UHV

Under UHV conditions, exposing cleaved, single-crystal NaCl(100) to laser fluences from 50 mJ/cm^2 up to the onset of plasma formation (typically 1.8 mJ/cm^2) produces readily detectable neutral emissions corresponding to ^{23}Na, ^{35}Cl, ^{37}Cl, and the four isotopic peaks of molecular Cl_2.[12] The intensity of the molecular chlorine signal is typically 80% of the atomic chlorine signal. Under the conditions of this work, the fragmentation of molecular chlorine in the ionizer increases the integrated signal at 35 amu/e by about 10%. Although this contribution is not strictly negligible, the effect on the shape of the most intense portion of the time-of-flight signal is small. Thus least-squares fits of Eq. (1) to the time-of-flight signals at 35 amu/e yield apparent temperatures similar to but slightly lower than those derived by fits to the corresponding signals at 23 amu/e, where the contribution of more massive species is truly negligible. In the work described below, we focus primarily on the atomic emissions.

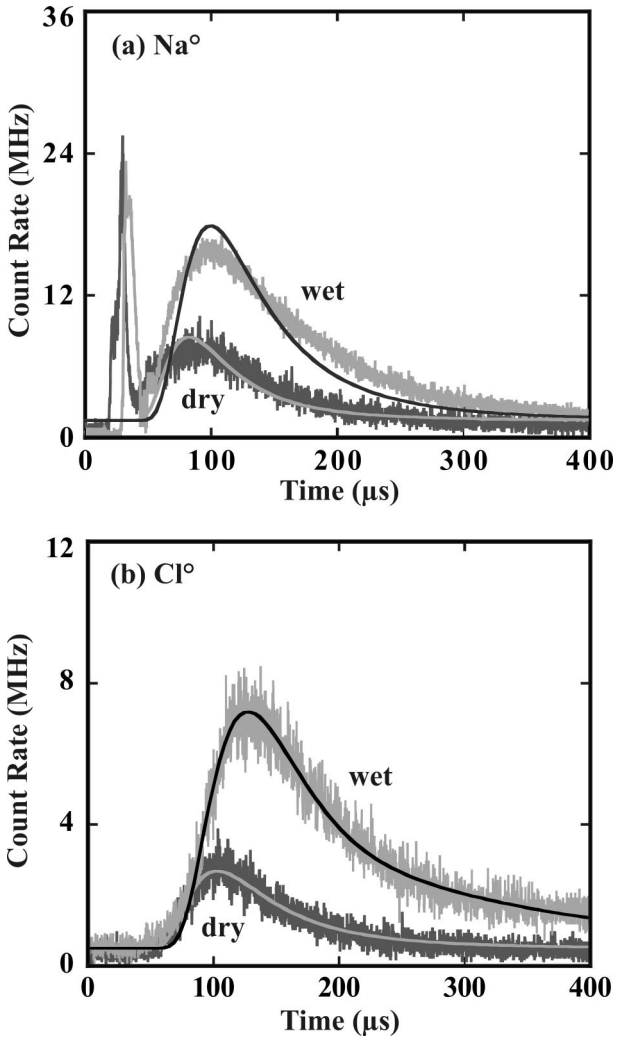

FIG. 1. Time-of-flight signals detected at (a) 23 amu/e (Na^0) and (b) 35 amu/e (Cl^0) during the irradiation of NaCl at a laser fluence of 120 mJ/cm^2 at a background sample temperature of 400 K. The signals labeled *dry* were acquired in UHV. The signals labeled *wet* were acquired in the presence of 10^{-5}-Pa water vapor.

B. Effect of water vapor on emission intensities

Time-of-flight signals for mass-selected emissions at 23 and 35 amu/e under UHV conditions (background pressure $<10^{-7}$ Pa) and in the presence of 10^{-5}-Pa water vapor are shown in Fig. 1. In each case, the background substrate temperature was 400 K and the laser fluence 120 mJ/cm^2. The first, narrow peak in the Na^0 emission at 30 μs corresponds to sodium emitted from the surface as positive ions.[16] For the purpose of analysis, this ion peak is neglected. Under UHV conditions, independent fits of Eq. (1) to the Na^0 and Cl^0 signals yield apparent temperatures of 2500 and 2350 K, respectively. Within experimental error, these temperatures are equal and are consistent with the thermal desorption of both species in thermal equilibrium with a heated substrate, where laser-induced heating has produced a transient temperature rise of about 2000 K. Simple heat loss calculations

indicate that the duration of this elevated temperature is quite short, on the order of tens of nanoseconds.[13] Thus, the duration of any thermally activated emission processes will be much less than the particle travel time (tens of microseconds), and the particle source may be treated as a delta function in time.[13]

As seen in Fig. 1, both emissions (Na^0 and Cl^0) are more intense in the presence of 10^{-5}-Pa water vapor. At any given fluence, both emissions show longer time of flights (slower velocities) in the presence of water vapor, indicating lower peak temperatures. Equation (1) provides a good description of the Cl^0 emissions under UHV conditions and in the presence of water vapor, and of the Na^0 emissions under UHV conditions. Although the Na^0 peak in the presence of water vapor is broader than the least-squares fit to Eq. (1), the resulting apparent temperature (1490 K) is nevertheless consistent with the (independently determined) apparent temperature derived from the Cl^0 data (1300 K). These temperature estimates suggest that the peak temperature produced by 120-mJ/cm^2 pulses in the presence of 10^{-5}-Pa water vapor is about 1400 K, 1000 K *less than the peak temperatures* under UHV conditions.

The presence of water vapor therefore reduces the magnitude of laser-induced heating in this material. Since the effect of water vapor is confined to the near-surface region, most of the laser-induced heating associated with these emissions can be attributed to laser absorption by near-surface defects, which we have recently confirmed.[13] This leads to the counterintuitive conclusion that water vapor both *increases* the emission intensities and *reduces* the defect densities. We address this issue below.

The effect of water vapor on emission intensity is especially clear when the total emission per laser pulse is integrated (i.e., area under the TOF curve) and plotted versus time. To improve the time resolution of these experiments, the laser-pulse repetition rate was increased to 5 Hz. This work employed a laser fluence of 120 mJ/cm^2 per pulse and a background substrate temperature of 500 K. Figure 2 shows the total counts per laser pulse detected at 23 amu/e (Na^0) prior to laser irradiation under UHV conditions ($t < 4$ s), during laser irradiation without water vapor ($t > 5$ s), and then during laser irradiation with water vapor ($t > 13.5$ s), where the partial pressure of water vapor was quickly increased to about 10^{-5} Pa. Over the course of one to two laser pulses (200–400 ms), the Na^0 signal increased by a factor of 5 [Fig. 2(b)]. This response is rate limited by the time required to open our leak valve. When the leak valve was closed at time $t=22$ s, the Na^0 signal showed an initial rapid drop of about 20%, followed by a long slow decay. Elevated Na^0 intensities are observed throughout the remainder of the experiment (for at least 18 s), despite the rapid drop in the water vapor pressure (over a few seconds).

The Na^0 signal in Fig. 2(b) displays a low-amplitude oscillation with a frequency of about 0.8 Hz. These oscillations are reproducible and are not associated with any known experimental artifact (e.g., fluctuations in laser intensity). Höche *et al.* and Szymonski *et al.* reported similar oscillations in the intensity of specularly reflected He atoms during vacuum ultraviolet (VUV) irradiation of single-crystal

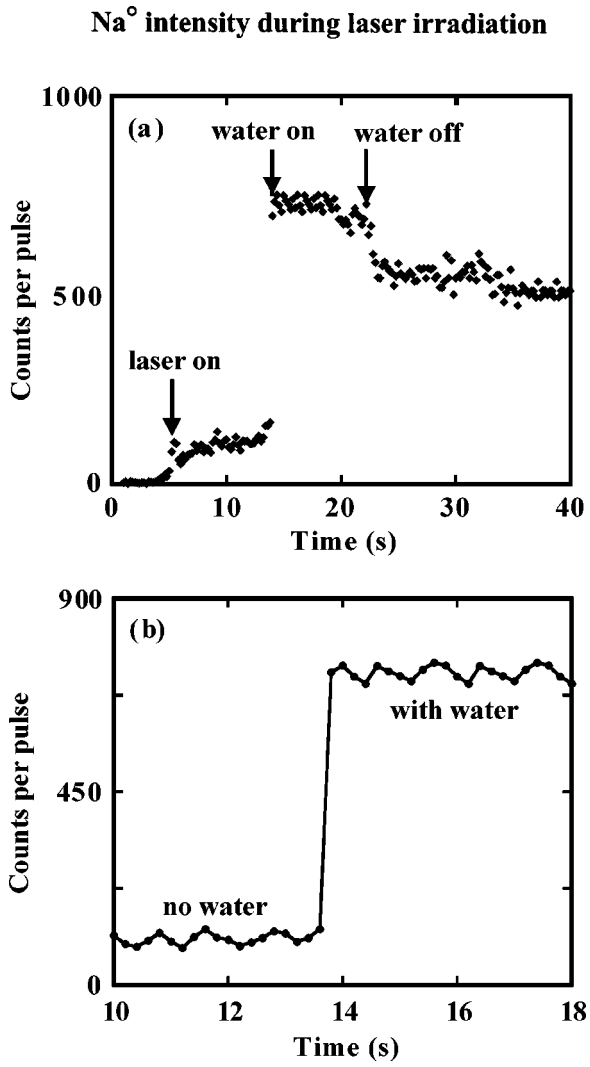

FIG. 2. (a) Pulse-to-pulse emission intensity detected at 23 amu/e (Na^0) during the irradiation of NaCl at a laser fluence of 120 mJ/cm^2 and a background sample temperature of 500 K. Irradiation commenced at time $t=4$ s under UHV conditions. At time $t=13.5$ s, a leak valve was smoothly opened, introducing degassed water vapor at a partial pressure of 10^{-5} Pa. The leak valve was smoothly closed at time $t=22$ s. (b) Expanded view of (a) showing the rise in emission intensity accompanying the introduction of water vapor.

NaCl.[9,11,17] These oscillations were attributed to cyclic variations in step and defect densities during layer-by-layer material removal, which in turn modulate the intensity of the specularly reflected He. Similar oscillations have been observed in the intensity of neutral particle emissions during the initial stages of electron-stimulated desorption from single-crystal KBr and NaCl.[18,19] These oscillations were also attributed to oscillations in the density of key structures, such as kinks along step edges, during layer-by-layer material removal. The oscillations we observe in Fig. 2 are most likely associated with a similar layer-by-layer material removal. Eventually, the formation of deeper etch pits, where the material is simultaneously removed from multiple levels, dampens these oscillations.

Measurements at 35 amu/e (Cl^0) from a different sample under comparable conditions are shown in Fig. 3. The effect of water vapor on the Cl^0 signal is similar to its

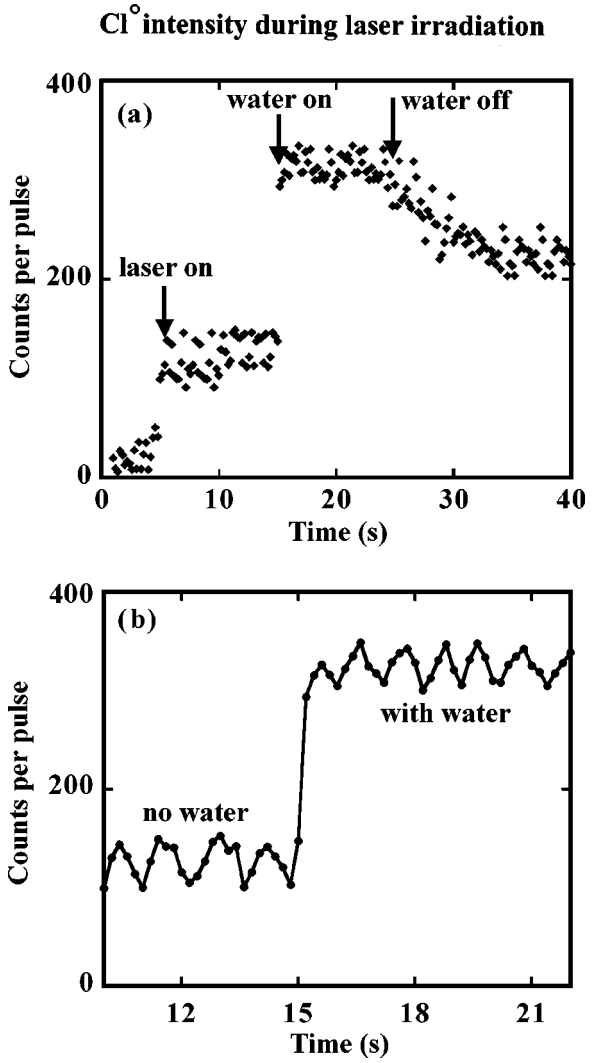

FIG. 3. (a) Pulse-to-pulse emission intensity detected at 35 amu/e (Cl^0) during the irradiaiton of NaCl at a laser fluence of 120 mJ/cm^2 and a background sample temperature of 500 K. Irradiation commenced at time t = 4 s under UHV conditions. At time t = 15 s, a leak valve was smoothly opened, introducing degassed water vapor at a partial pressure of 10^{-5} Pa. The leak valve was closed at time t = 23 s. (b) Expanded view of (a) showing the rise in emission intensity accompanying the introduction of water vapor.

effect on the Na^0 signal, although somewhat smaller. Rapidly introducing 10^{-5}-Pa water vapor increases the Cl_0 signal by a factor of 3 over the course of one or two laser pulses. The Cl^0 signal in Fig. 3 oscillates with a frequency of about 1.1 Hz. The small difference in the oscillation frequencies of Figs. 2 and 3 is presumably due to small differences in the sample and irradiation conditions. Again, layer-by-layer desorption is the most likely explanation for these oscillations.

A comparison of the steady-state intensities (after induction) of the three most important neutral signals at four values of water vapor partial pressure is shown in Fig. 4. In general, water vapor increases the fraction of chlorine detected as Cl_2^0. The ratio of total sodium to total chlorine is about 0.8 ± 0.3, indicating a nearly stoichiometric material removal. In the presence of water vapor, weak signals at 1 amu/e (H^0) and 16 amu/e (O^0) are also observed. The desorption of H^0 and O^0 is observed during electron irradiation of chemisorbed water on oxide surfaces.[20] Little work has been done on laser desorption of dissociation products of chemisorbed water on similar surfaces.

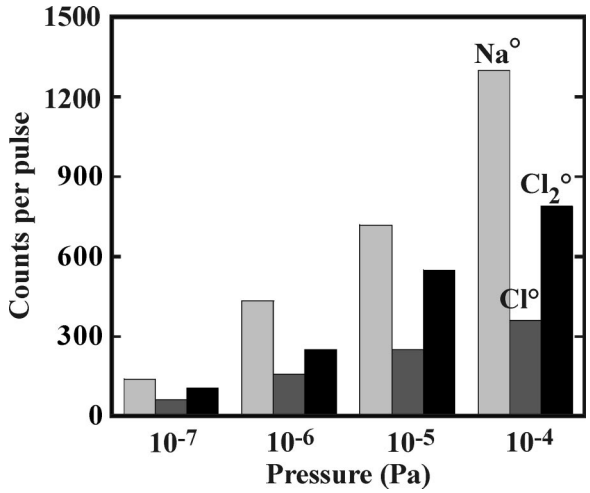

FIG. 4. Relative intensities of the three principal neutral emissions detected during laser irradiation at a fluence of 120 mJ/cm^2 and a background sample temperature of 400 K under UHV conditions (total pressure $<10^{-7}$ Pa) and in the presence of 10^{-6}-, 10^{-5}-, and 10^{-4}-Pa water vapor.

C. Effect of background substrate temperature

Raising the background temperature of the sample with a resistance heater increases the intensity of the Na^0 and Cl^0 emissions and shifts the peak time of flight to shorter times. Time-of-flight signals at 35 amu/e (Cl^0) detected in the presence of 10^{-5}-Pa water vapor at background substrate temperatures of 400, 600, and 800 K at a fluence of 120 mJ/cm^2 are shown in Fig. 5. The corresponding translational temperatures derived from curve fits to Eq. (2) are roughly 1500, 1700, and 1900 K, respectively, consistent with a laser-induced temperature rise of 1100 K above the background temperature in each case. Although this result is not surprising, we believe this is a direct experimental evidence that the apparent temperature of the emissions is equal to the *sum* of

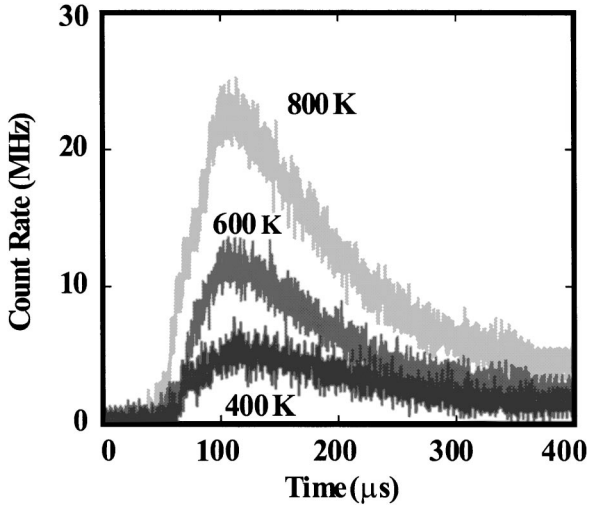

FIG. 5. Time-of-flight signals detected at 35 amu/e (Cl^0) detected at a fluence of 120 mJ/cm^2 in the presence of 10^{-5}-Pa water vapor and at background sample temperatures of 400, 600, and 800 K.

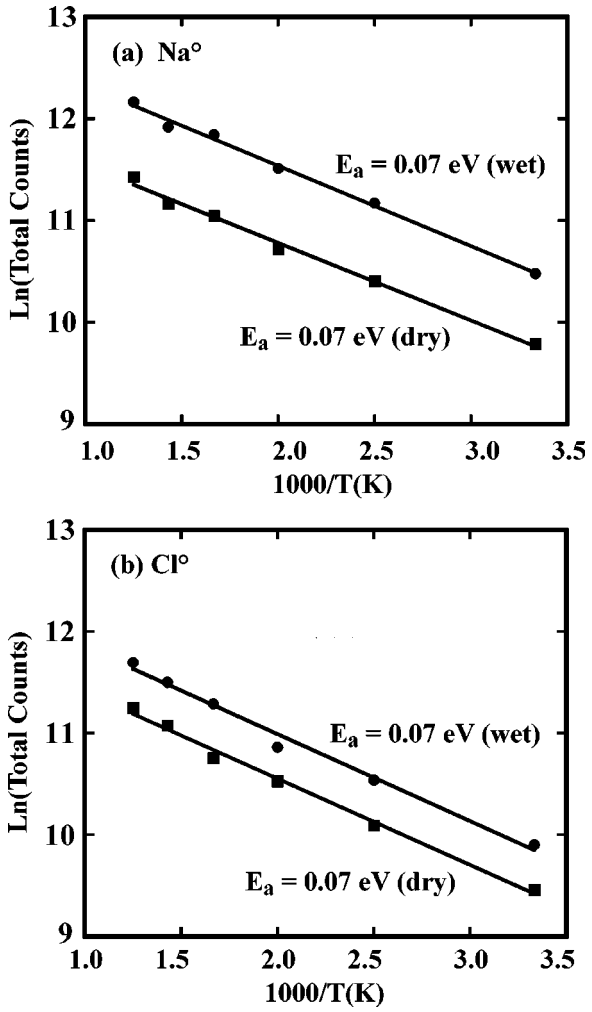

FIG. 6. Arrhenius plots of the emission intensities detected at (a) 23 amu/e (Na^0) and (b) 35 amu/e (Cl^0) vs background sample temperature during laser irradiation at a fluence of 120 mJ/cm^2 under UHV conditions (lower curves) and in the presence of 10^{-5}-Pa water vapor (upper curves).

the surface background temperature and the laser-induced temperature change.

Figure 6 shows Arrhenius plots of the Na^0 and Cl^0 intensities at a fixed laser fluence of 120 mJ/cm^2 as a function of background substrate temperature under UHV conditions (dry) and in the presence of 10^{-5}-Pa water vapor (wet). In each case, the signals display Arrhenius behavior corresponding to the same activation energy $E_a = (0.07 \pm 0.005)$ eV. Water vapor has no significant effect on this activation energy. As discussed below, this activation energy is consistent with the activation energy associated with bulk *F-H* pair generation via thermally assisted, photoelectronic excitation.[2] This process is initiated by a two-photon excitation to produce a self-trapped exciton, followed by the thermally assisted motion of a chlorine atom to an adjacent lattice site to form an *F-H* pair. Many other cation and anion defect structures subsequently form (*V* centers, H_2 centers, *I* centers, *H*-center aggregates)[21] depending upon the excitation density, crystal temperature, and other factors. The complex bulk behavior can then lead to particle emission following the diffusion of "active" defect species to the crystal surface. The kinetics would be expected to follow the

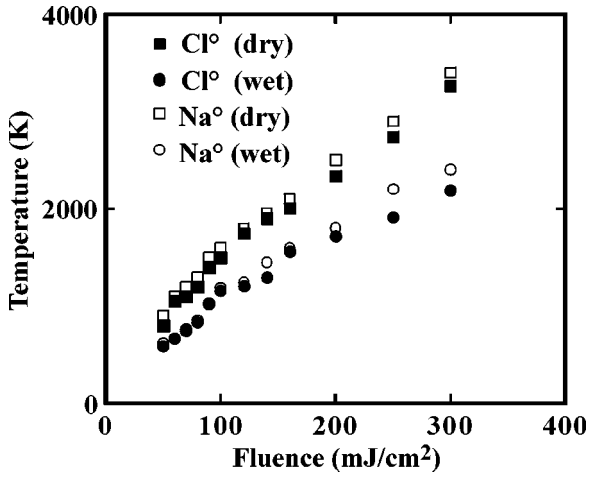

FIG. 7. Peak surface temperatures derived from Maxwell–Boltzmann fits to the time-of-flight signals detected at (a) 23 amu/e (Na^0) and (b) 35 amu/e (Cl^0) vs laser fluence under UHV conditions (dry) and in the presence of 10^{-5}-Pa water vapor (wet). The background sample temperature was 300 K.

background substrate temperature (as opposed to the peak laser-induced temperature) if the defect formation occurs within the bulk sample below the strongly heated surface layer.

D. Effect of laser-induced heating

At a constant background substrate temperature, raising the laser fluence both increases the emission intensities and shifts the time-of-flight peaks to shorter times (Fig. 1). Both effects are consistent with an emission mechanism that is promoted by transient surface heating during the laser pulse. Figure 7 shows the temperatures determined by fitting the time-of-flight curves to Eq. (1) versus laser fluence for both Na^0 and Cl^0 under UHV conditions and in the presence of 10^{-5}-Pa water vapor at a background substrate temperature of 300 K. As expected, the temperatures in Fig. 7 are significantly lower in the presence of water vapor. This suggests that the presence of water vapor reduces the amount of laser energy absorbed near the sample surface.

The temperature increase with fluence in Fig. 7 is nearly linear. In a recent work, we showed that a substantial fraction of the laser energy is absorbed in the near-surface region to account for these high temperatures.[13] This absorption develops over the first five or ten laser pulses and then saturates. The reflectance spectra acquired after irradiation suggest that the absorption near 248 nm is due to high densities of *V*-type centers in the near-surface region. The deviation of the peak temperature versus fluence from a linear behavior at the higher fluencies in Fig. 7 can be attributed to saturation in the laser-induced absorption (i.e., induced defect density) with increasing fluence.[13]

Pulse-to-pulse measurements of laser absorption at 248 nm show a dramatic increase in absorption in the early stages of irradiation. Figure 8 shows the results of absorption measurement during the first 20 laser pulses (100 mJ/cm^2) under UHV conditions and in the presence of 10^{-5}-Pa water vapor. In both cases, the laser absorbance grows from low values over the first several pulses. In the presence of water vapor,

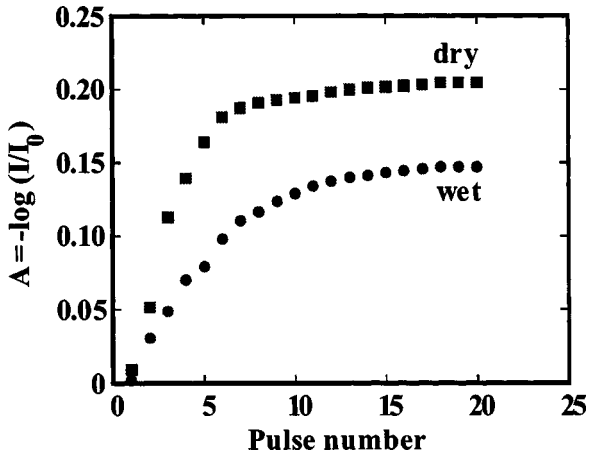

FIG. 8. Pulse-to-pulse measurements of the absorbance $[\log_{10}(I_0/I)]$ at 248 nm at a fluence of 100 mJ/cm^2 under UHV conditions (dry) and in the presence of 10^{-5}-Pa water vapor (wet). In both cases, the absorption rises from low values during the first five or ten laser pulses. After 20 laser pulses, the absorption in the presence of water vapor is about 30% less than the absorption measured under UHV conditions.

the absorbance after 20 laser pulses is clearly lower than the absorbance measured under UHV conditions. This absorbance change corresponds to a 30% drop in the absorbed laser energy in the presence of water vapor. Simplistically, this should decrease the temperature change in the presence of water vapor by 30%. This is consistent with the observed temperature difference (~25%) inferred from the time-of-flight data at the same fluence due to the presence of water vapor (1500 K under UHV conditions versus 1200 K in the presence of water vapor).

The low initial absorption of NaCl at 248 nm in Fig. 8 is consistent with the high transparency of intrinsic NaCl at 248 nm. During and immediately after each laser pulse, any weak emission during the initial stages of irradiation will have little effect on the observed time-of-flight curves. Due to the strong temperature dependence of thermal emissions, the total emission intensities are dominated by particles emitted at the highest surface temperatures.[13] Thus the apparent surface temperatures in Fig. 7 reflect the peak surface temperatures achieved after the laser absorption saturates, when the highest temperatures are reached.

The variation of Na^0 and Cl^0 intensities with the apparent peak temperature under UHV conditions and in the presence of 10^{-5}-Pa water vapor at a background substrate temperature of 300 K are shown in Fig. 9. In each case, the emission intensities increase in a nonlinear fashion with increasing temperature, suggesting a thermal, rate-limiting step.[22–25] The same intensity data are displayed in Arrhenious form in Fig. 10 using the temperature derived from the corresponding time-of-light curves. The intensity variations with temperature are consistent with a thermally assisted process with activation energies of 0.29–0.30 eV under UHV conditions and 0.19–0.20 eV in the presence of 10^{-5}-Pa water vapor. Both activation energies are much greater than the 0.07 eV associated with changes in the background sample temperature.

The activation energies observed under UHV conditions correspond closely to the (0.27 ± 0.02) eV activation energy

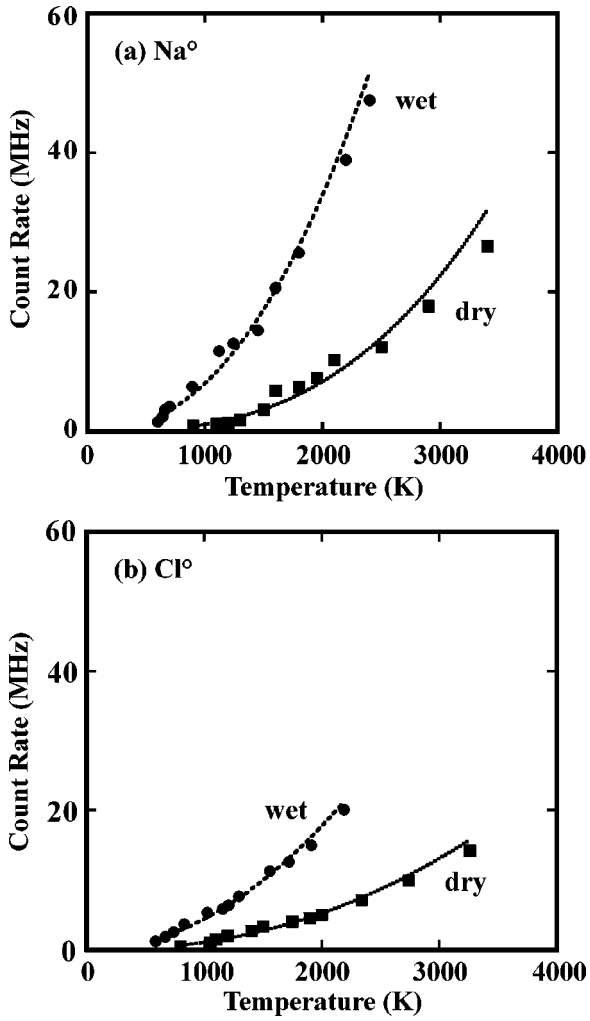

FIG. 9. Emission intensities detected at (a) 23 amu/e (Na^0) and (b) 35 amu/e (Cl^0) vs peak surface temperature derived from Maxwell–Boltzmann fits to the corresponding time-of-flight signals at a background sample temperature of 300 K. The points labeled *dry* represent intensities measured under UHV conditions. The points labeled *wet* represent intensities measured in the presence of 10^{-5}-Pa water vapor.

observed by Höche *et al.* for the layer-by-layer removal of NaCl exposed to light from a deuterium lamp under UHV conditions at temperatures below 390 K.[9] Emissions under pulsed UV laser radiation appear to be rate limited by a similar process, despite the fact that the temperatures during emission can be thousands of kelvin higher.[13]

In the presence of 10^{-5}-Pa water vapor, the apparent activation energies are lower, 0.19–0.20 eV (Fig. 10). This significant decrease in activation energy accounts for the especially intense emissions in the presence of water vapor, despite the lower apparent surface temperatures. Since the effect of water vapor is largely confined to the surface, we propose that the 0.2–0.3-eV thermally assisted process affected by water takes place principally along the sample surface. In contrast, the 0.07-eV process associated with the background substrate temperature is not affected by water vapor, consistent with a process taking place in the sample interior.

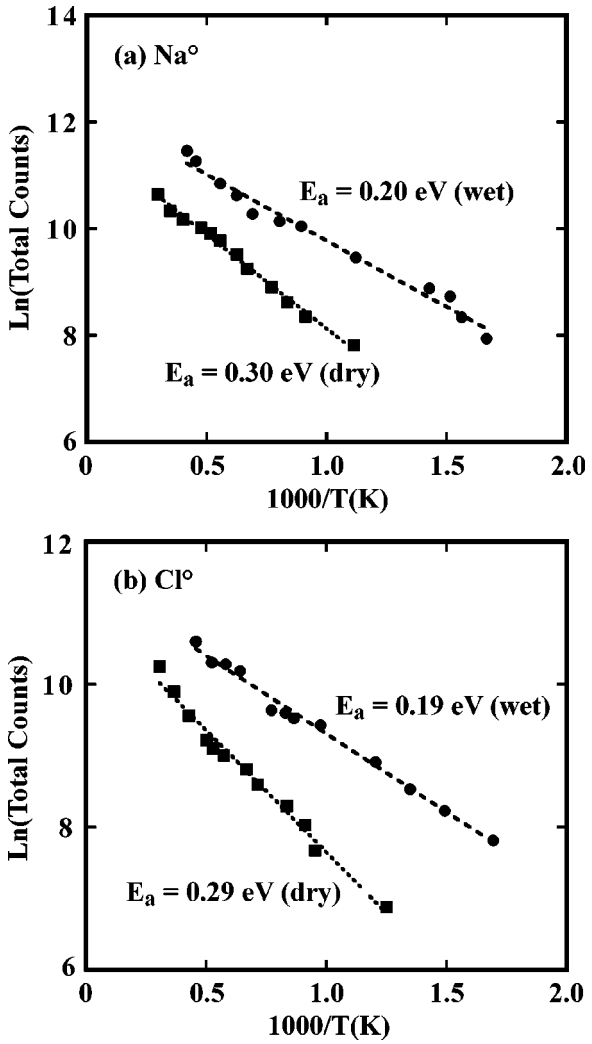

FIG. 10. Arrhenius plots of the emission intensities detected at (a) 23 amu/e (Na^0) and (b) 35 amu/e (Cl^0) vs peak surface temperature derived from Maxwell–Boltzmann fits to the corresponding time-of-flight signals under UHV conditions (dry) and in the presence of 10^{-5}-Pa water vapor (wet) at a background sample temperature of 300 K.

E. Effect of water on surface topography

The amount of material removed as neutral particles is consistent with significant surface erosion. Under UHV conditions, the small surface modifications can be imaged by *ex situ* atomic force microscopy (AFM). AFM images of a cleaved NaCl(100) surface irradiated under UHV conditions at a background temperature of 300 K are shown in Figs. 11(b)–11(d). For comparison, an image of the same sample acquired outside the irradiated area is shown in Fig. 11(a). Outside the irradiated region, the sample shows relatively smooth atomic steps 0.29 nm in height, typical of cleaved NaCl. Figure 11(b) shows a region of the surface exposed to 50 laser pulses at a fluence of 80 mJ/cm^2. This treatment produces irregular islands distributed rather uniformly across the surface except near cleavage steps, where the island density is reduced. The average island step height of (0.29 ± 0.02) nm is consistent with the 0.29-nm steps of single NaCl monolayers. This value is inconsistent with metallic Na monolayers[26] or NaOH monolayers[27] both of which would yield significantly higher steps. Nearby cleavage steps in this and other images are strongly eroded, suggesting that the islands are formed of NaCl desorbed from nearby cleavage steps. Significantly, such island formation is not observed on surfaces exposed to energetic electron beams either in our laboratory or in others.[10] The high temperatures produced by pulsed laser radiation appear to be necessary for island formation.

Images of surfaces exposed to the same number of pulses at a somewhat higher laser fluence of 120 mJ/cm^2 are shown in Figs. 11(c) and 11(d). At this higher fluence, the total island area is somewhat lower. In addition, this treatment produces detectable monolayer-deep etch pits. Comparing surfaces exposed to lower fluences, as in Fig. 11(b), with surfaces exposed to higher fluences, as in Figs. 11(c) and 11(d), suggests that the islands appear before the pits. Therefore, we cannot attribute the observed islands to material left behind from extensive monolayer desorption and pit formation. Instead, we attribute the islands to aggregates of material removed from eroding steps.

The laser-induced pits in Figs. 11(c) and 11(d) are similar to monolayer-deep etch pits produced by exposure to continuous electron and UV radiation on KBr (Refs. 10, 11, 18, and 28) and KI (Ref. 29) surfaces at elevated temperatures. We have recently showed that exposing NaCl to 2-keV electrons at room temperature generates rounded pits similar to those in Figs. 11(c) and 11(d). Following Szymonski *et al.*, we attribute the pits produced by pulsed 248-nm radiation to F-center aggregation at the surface. The majority of these F centers are created in the sample interior and subsequently diffuse to the surface. Diffusing F centers are expected to emerge preferentially along preexisting surface steps.[30] Therefore, once a pit is nucleated, F center diffusion from below gradually increases its size. Steps tend to deplete the nearby subsurface region of mobile F centers, hindering pit nucleation and growth near preexisting steps. This would account for the small number of monolayer pits near cleavage steps in Figs. 11(c) and 11(d).

The more intense emission in the presence of water vapor results in correspondingly larger topographical changes on the exposed surface. In the presence of 10^{-5}-Pa water vapor, surfaces exposed to 50 laser pulses at 120 mJ/cm^2 were too rough to be imaged by AFM. A scanning electron microscope (SEM) image of such a surface is shown in Fig. 12. Although much of the surface is devoid of features at this resolution (AFM shows it to be very rough), the image shows micron-sized pits that are hundreds of nanometers deep. The volume of these deep pits is consistent with estimates of the amount of material removed by emission processes in the presence of 10^{-5}-Pa water vapor. Especially rapid surface erosion would deplete the surface of point defects and help account for reduced laser absorption and lower apparent surface temperatures in the presence of water vapor.

IV. DISCUSSION

A. Emission mechanism in UHV

Several laser-induced effects are responsible for the emission and topographical changes observed during the 248-nm radiation reported above. Both structural and point

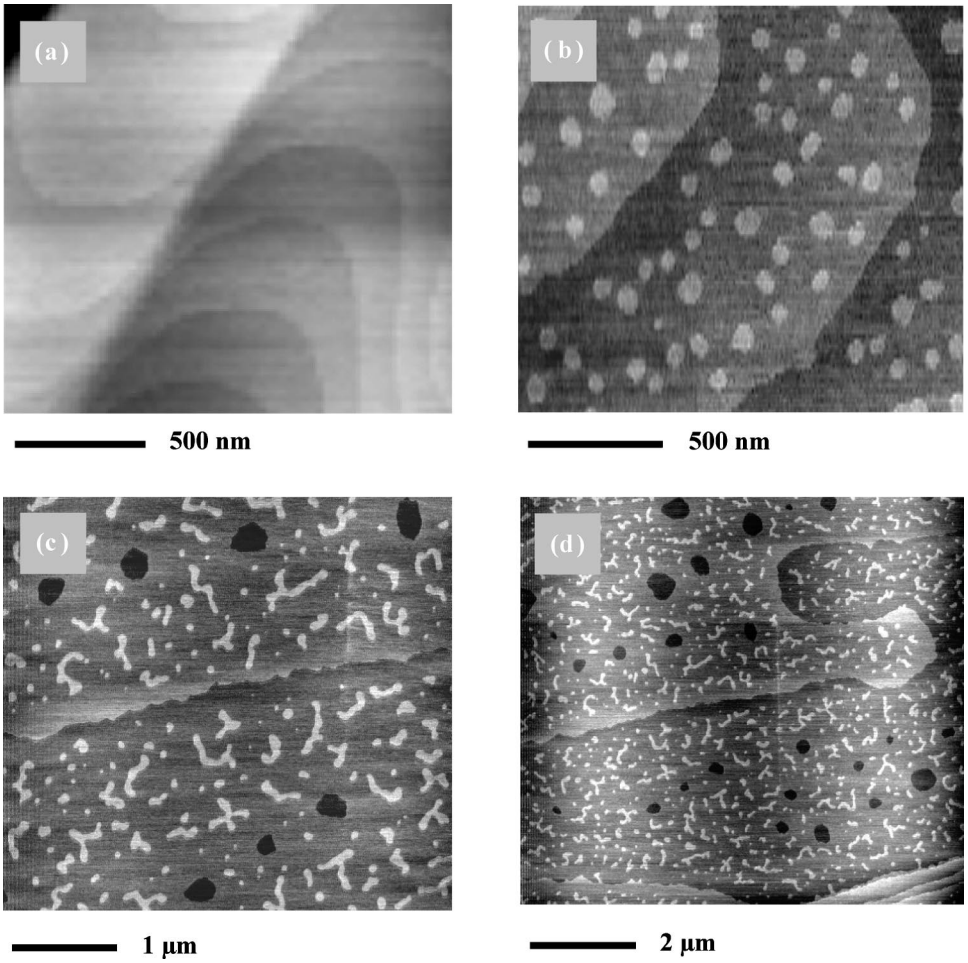

FIG. 11. AFM images of cleaved NaCl(100) surfaces: (a) not exposed to the 248-nm radiation, showing typical smooth, monolayer-high cleavage steps; (b) exposed to 50 pulses at a laser fluence of 80 mJ/cm^2 under UHV conditions; (c) exposed to 50 pulses at a laser fluence of 120 mJ/cm^2 under UHV conditions; and (d) a larger image of the surface shown in (c). Laser irradiation was performed at a background substrate temperature of 300 K.

defects play important roles. The 0.07-eV activation energy for emission as a function of the sample background temperature suggests that *F-H* pair production, presumably by two-photon absorption in the bulk, is a rate-limiting step in emission.[12,31] The diffusion of *F* centers to the surface is most likely responsible for pit nucleation and growth as well as step roughening, both observed in the AFM images of irradiated surfaces in Figs. 11(b)–11(d).

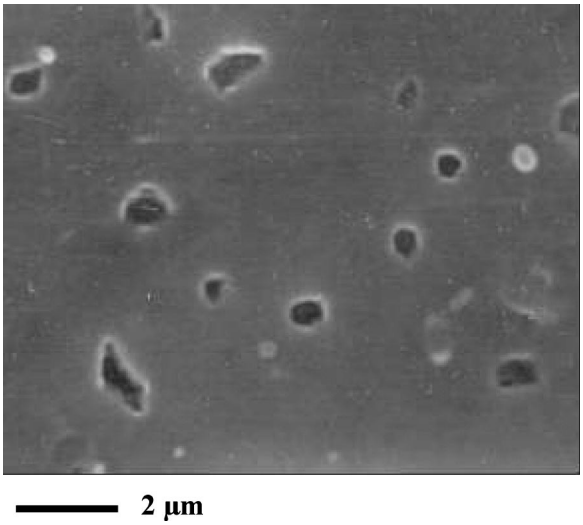

FIG. 12. SEM image of a NaCl(100) surface exposed to the 50 laser pulses at a fluence of 120 mJ/cm^2 in 10^{-5}-Pa water vapor at a background substrate temperature of 300 K.

Neutral emission is strongly affected by laser-surface heating. We have recently identified a strong, near-surface absorption at 248 nm due to *V* centers, which are formed when *H* centers are trapped at near-surface defects.[12] This absorption grows over several laser pulses and is sufficient to account for the high apparent temperatures of the accompanying atomic emissions. The growth of absorption at 248 nm is accompanied by a comparable growth in atomic emission intensities (induction or incubation).

The role of diffusion along the steps in the production of atomic emissions is suggested by the 0.30-eV activation energy observed as a function of the apparent emission temperatures.[12] A similar apparent activitation energy was associated by Höche *et al.* with the shuffling of ions along the steps in NaCl previously exposed to UV radiation to induce step roughening.[9]

The diffusion of ions along the ⟨100⟩ steps is complicated by the checkerboard pattern of electrostatic potentials along the surfaces of rocksalt structure materials, illustrated in Fig. 13. Moving an isolated ion along a step (left) involves a high-energy intermediate state one nearest-neighbor distance from the step—essentially equivalent to a terrace site. In contrast, an ion pair (right) can diffuse by a shuffling motion, with a much lower energy intermediate state. This intermediate state is nevertheless vulnerable to detachment, e.g., by photoinduced electron or hole transfer, generating neutral species. Sushko *et al.* have shown that the band gap for ionic crystals is significantly reduced at low coordinated

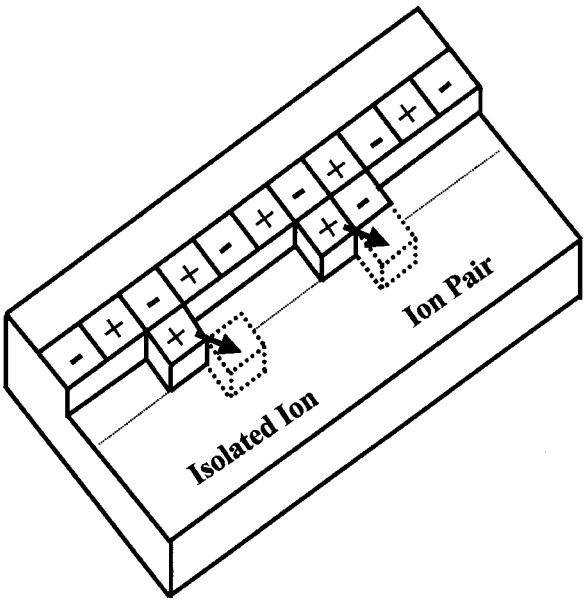

FIG. 13. Schematic model of ion diffusion along a ⟨100⟩ step on a NaCl(100) surface. The diffusion of isolated ions is hindered by the large energy required to separate the single ion from the step. The diffusion of ion pairs requires less energy, as each ion maintains at least two nearest neighbors of the opposite sign. We propose that photoelectronic excitation of the transient structure on the right (shown schematically by the dotted lines) can remove the outermost ion from the step—ejecting it either into vacuum (as a neutral particle) or onto nearby terrace sites (as an ion).

sites, such as steps and kinks, making photoelectronic release of electrons due to single 248-nm excitations a strong possibility.[32,33] These neutrals can then undergo thermal desorption, either into vacuum or onto terrace sites. In this scenario, the neutral emission intensities are rate limited by the number of vulnerable ions, which depends critically on the diffusion rate. Thus, the Arrhenius analysis of the neutral emission intensities yields the value associated with this diffusion, namely, 0.30 eV. This process accounts for the desorption of both Na^0 and Cl^0. Aggregation of neutral species emitted onto terrace sites would form the observed islands.

B. Effect of water on emission process

Under normal conditions, water does not react significantly with nondefective NaCl(100) surfaces. When water vapor is deposited on clean NaCl(001) surfaces at low temperatures (<130 K), it virtually all desorbs upon heating to 160 K.[34,35] Fölsch and Henzler show evidence that water remaining on surfaces heated to 160 K is absorbed at defect sites, such as surface steps.[35] X-ray photoelectron signals due to molecular water at the steps disappear upon further heating to room temperature. Importantly, electron-irradiated surfaces dosed with water at 130 K and then heated to room temperature showed strong evidence for OH^+ species absorbed at surface chlorine vacancies (*F* centers).[35] Related surface defects associated with water-derived protons have been identified in cubic MgO,[36,37] and may play a role in NaCl a well. Dissociative absorption of water molecules at defects is expected to play an important role in the emission of neutral atoms and molecules in the presence of water vapor.

The activation-energy measurements of Fig. 10 suggest that the presence of 10^{-5}-Pa water vapor acts to lower the activation of the 0.30-eV process that limits emission under UHV conditions. We propose that the high polarizability of the water molecule ion would tend to shield nearby Na^+ and Cl^- ions from the electric fields applied by the nearby lattice. This would reduce the energy required for diffusion along steps, and thus decrease the activation energy for the formation of vulnerable defect configurations.

The rapid response of the emission intensities to the introduction of water vapor (<1 s) requires some explanation. At a partial pressure of 10^{-5}-Pa, any given surface site will be struck by a water molecule from the nearby vacuum on the average of once every 10 s. If every water molecule striking the surface adsorbed and remained at the point of first contact (sticky molecule approximation), the time constant for water interactions would be on the order of 10 s. This is much longer than the time constant for water effects in this work—less than 1 s at a partial pressure of 10^{-5} Pa. Much faster responses are possible if each adhering water molecule visits a large number of sites before adsorbing tightly at a defect site or desorbing back into vacuum.

The SEM image of Fig. 12 shows a relatively smooth surface with several deep etch pits. This requires that the surface preferentially erodes near the bottom of preexisting pits; that is, the pits tend to grow down instead of out. Although we have not examined the pit cross sections in detail, the water-laser combination appears to favor directional etching—an often desirable trait. This behavior can be rationalized if the erosion of multilayer steps is hindered. In this case, pits nucleated along the bottom of a deep structure can grow only as wide as the pit immediately above it.

The deep pits in Fig. 12 suggest that the total number of surface steps participating in the emission processes does not change greatly during the course of irradiation—several tens of laser pulses at this fluence. Although some change is expected, dramatic changes would complicate the analysis of intensity measurements as a function of surface treatment. The validity of the Arrhenius relation in particular requires that the population of the initial states remains constant as the temperature changes. If erosion is limited to the bottom of preexisting pits, as suggested above, the average number and length of eroding steps would tend to remain constant. This would also limit the fraction of surface sites participating in the emission. Under these conditions, which yield especially rapid erosion, the effect of water on erosion rates may well be underestimated.

V. CONCLUSION

Under a 248-nm laser radiation, cleaved, single-crystal NaCl yields significant atomic emissions of Na^0 and Cl^0. These emissions involve at least two thermally activated steps. A low activation-energy process (0.07 eV) takes place primarily in the bulk of the sample at temperatures near the background sample temperature. We associate this process with *F-H* pair production accompanying two-photon excitation across the band gap, followed by electron-hole recombination. The subsequent diffusion of *F* centers to the surface

nucleates kinks along steps and pits along terraces which participate in subsequent emission processes. A high activation-energy process (0.30 eV in UHV) takes place primarily along the surface due to ion diffusion along the steps. Intermediate states associated with step diffusion are expected to be weakly bound. We propose that photoelectronic excitation of these weakly bound states by 248-nm photons ejects the vulnerable particles either directly into vacuum or onto nearby terrace sites.

Low partial pressures of water vapor ($\sim 10^{-5}$ Pa) dramatically increase the rates of laser-induced neutral emission and surface erosion, especially at elevated background sample temperatures. We attribute these effects to a water-induced decrease in the activation energy for step diffusion, most likely involving sorbed OH^-.[35,38] The effect of water on laser-induced neutral emission and surface erosion in sodium chloride is analogous to the effect of reactive gases on plasma etching in the semiconductor industry. In the case of sodium chloride, water and its dissociation products play the role of the fluorine ions produced by the dissociation of fluorine-containing species in the plasma etching of silicon oxide.

Many geological and biological materials display strong interactions with polar water molecules and may display similar vapor-enhanced emissions under laser radiation. These interactions may prove important in the use of laser desorption and ablation for environmental analysis and the generation of nanostructured surfaces. An understanding of these effects should provide additional tools for the control of laser interactions in this important class of materials.

ACKNOWLEDGMENTS

This work was supported by the Department of Energy Division of Chemical Sciences of the Office of Basic Energy Sciences including Contract No. DE-FG02-04ER15618. Pacific Northwest National Laboratory is operated for the U.S. Department of Energy by Battelle under Contract No. DE-AC06-76RLO 1830. We thank Alexander Shluger, University College London, for many helpful discussions, and Carsten Seiler, Washington State University, for acquiring the AFM images.

[1]F. Seitz, Rev. Mod. Phys. **26**, 7 (1954).
[2]N. Itoh, Adv. Phys. **31**, 491 (1982).
[3]R. T. Williams, Radiat. Eff. Defects Solids **109**, 175 (1989).
[4]N. Itoh and A. M. Stoneham, *Materials Modifications by Electronic Excitation* (Cambridge University Press, New York, 2001).
[5]A. Schmid, P. Bräunlich, and P. K. Rol, Phys. Rev. Lett. **35**, 1382 (1975).
[6]P. D. Townsend, R. Browning, D. J. Garlant, J. C. Kelly, A. Mahjoobi, A. J. Michael, and M. Saidoh, Radiat. Eff. **30**, 55 (1976).
[7]W. P. Hess, A. G. Joly, D. P. Gerrity, K. M. Beck, P. V. Sushko, and A. L. Shluger, J. Chem. Phys. **115**, 9463 (2001).
[8]T. Kubo, A. Okano, J. I. Kanasaki, K. I. Ishikawa, Y. Nakai, and N. Itoh, Phys. Rev. B **49**, 4931 (1994).
[9]H. Höche, J. P. Toennies, and R. Vollmer, Phys. Rev. B **50**, 679 (1994).
[10]B. Such, P. Czuba, P. Piatkowski, and M. Szymonski, Surf. Sci. **451**, 203 (2000).
[11]M. Szymonski, J. Kolodziej, B. Such, P. Piatkowski, P. Struski, P. Czuba, and F. Krok, Prog. Surf. Sci. **67**, 123 (2001).
[12]K. H. Nwe, S. C. Langford, and J. T. Dickinson, J. Appl. Phys. (in press).
[13]K. H. Nwe, S. C. Langford, and J. T. Dickinson, J. Appl. Phys. **97**, 043502 (2005) (preceding article).
[14]Y. Kawaguchi, M. L. Dawes, S. C. Langford, and J. T. Dickinson, J. Appl. Phys. **89**, 2370 (2001).
[15]P. A. Redhead, J. P. Hobson, and E. V. Kornelsen, *The Physical Basis for Ultrahigh Vacuum* (Chapman and Hall, London, 1967).
[16]C. Bandis, S. C. Langford, and J. T. Dickinson, Appl. Phys. Lett. **76**, 421 (2000).
[17]H. Höche, J. P. Toennies, and R. Vollmer, Phys. Rev. Lett. **71**, 1208 (1993).
[18]B. Such, J. Kolodziej, P. Czuba, P. Piatkowski, P. Struski, F. Krok, and M. Szymonski, Phys. Rev. Lett. **85**, 2621 (2000).
[19]B. Such, J. Kolodziej, F. Krok, P. Struski, P. Piatkowski, and M. Szymonski, Radiat. Eff. Defects Solids **156**, 69 (2000).
[20]M. Akbulut, N. J. Sack, and T. E. Madey, Surf. Sci. **351**, 209 (1996).
[21]D. E. Aboltin, V. J. Grabovskis, A. R. Kangro, C. Lushchik, A. A. O'Konnel-Bronin, I. K. Vitol, and V. E. Zirap, Phys. Status Solidi A **47**, 667 (1978).
[22]J. T. Dickinson, J.-J. Shin, W. Jiang, and M. G. Norton, J. Appl. Phys. **74**, 4729 (1993).
[23]R. L. Webb, S. C. Langford, and J. T. Dickinson, Nucl. Instrum. Methods Phys. Res. B **103**, 297 (1995).
[24]R. L. Webb, T. Lippert, S. C. Langford, and J. T. Dickinson, Appl. Surf. Sci. **127–129**, 815 (1998).
[25]T. Lippert, S. C. Langford, A. Wokaun, G. Savas, and J. T. Dickinson, J. Appl. Phys. **86**, 7116 (1999).
[26]H. Häkkinen and M. Manninen, J. Chem. Phys. **105**, 10565 (1996).
[27]R. W. G. Wyckoff, *Crystal Structures*, 2nd ed. (Interscience, New York, 1963), Vol. 1.
[28]R. Bennewitz *et al.*, Surf. Sci. **474**, L197 (2001).
[29]R. M. Wilson, W. E. Pendleton, and R. T. Williams, Radiat. Eff. Defects Solids **128**, 79 (1994).
[30]V. Puchin, A. Shluger, Y. Nakai, and N. Itoh, Phys. Rev. B **49**, 11364 (1994).
[31]K. H. Nwe, S. C. Langford, and J. T. Dickinson, Appl. Surf. Sci. **197–198**, 83 (2002).
[32]P. V. Sushko, J. L. Gavartin, and A. L. Shluger, J. Phys. Chem. B **101**, 2269 (2002).
[33]P. V. Sushko and A. L. Shluger, Surf. Sci. **421**, L157 (1999).
[34]J. Estel, H. Hoinkes, H. Kaarmann, H. Nahr, and H. Wilsch, Surf. Sci. **54**, 393 (1976).
[35]S. Fölsch and M. Henzler, Surf. Sci. **247**, 269 (1991).
[36]D. Ricci, C. Di Valentin, G. Pacchioni, P. V. Sushko, A. L. Shluger, and E. Giamello, J. Am. Chem. Soc. **125**, 738 (2002).
[37]D. Ricci, G. Pacchioni, P. V. Sushko, and A. Shluger, J. Chem. Phys. **117**, 2844 (2002).
[38]D. J. Dai, S. J. Peters, and G. E. Ewing, J. Phys. Chem. **99**, 10299 (1995).